"Triple-Punch" Strategy for Triple Negative Breast Cancer Therapy with Minimized Drug Dosage and Improved Antitumor Efficacy

Shishuai Su,[†] Yanhua Tian,[†] Yiye Li,[†] Yanping Ding, Tianjiao Ji, Meiyu Wu, Yan Wu,[*] and Guangjun Nie[*]

CAS Key Laboratory for Biomedical Effects of Nanomaterials and Nanosafety, National Center for Nanoscience and Technology of China, No. 11 Beiyitiao, Zhongguancun, Beijing 100190, China. [†]These authors contributed equally to this work.

ABSTRACT Effective therapeutics against triple negative breast cancer (TNBC), which has no standard-of-care therapy, needs to be developed urgently. Here we demonstrated a strategy of integrating indocyanine green (ICG), paclitaxel (PTX), and survivin siRNA into one thermosensitive poly(2-(2-methoxyethoxy)ethyl methacrylate-*co*-oligo(ethylene glycol) methacrylate)-*co*-2-(dimethylamino)ethyl methacrylate-*b*-poly(D,L-lactide-*co*-glycolide) (P (MEO_2MA-*co*-OEGMA-*co*-DMAEMA)-*b*-PLGA) nanoparticle (NP-IPS) for triple-punch strategy against TNBC. The NP-IPS significantly enhanced the stability of ICG. Controlled release of the PTX in tumor regions was triggered by the hyperthermia produced by laser irradiated ICG. The NP-IPS exhibited remarkable antitumor efficacy (almost complete ablation of the tumor xenografts) due to the combinational effects of chemotherapy, photothermal therapy, and gene therapy with low drug dose (ICG, 0.32 μmol/kg; PTX, 0.54 μmol/kg; siRNA, 1.5 mg/kg) and minimal side effects. Taken together, our current study demonstrates a nanoplatform for triple-therapy, which reveals a promising strategy for TNBC treatment.

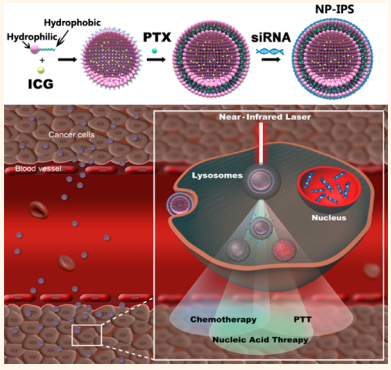

KEYWORDS: thermoresponsive · triple negative breast cancer · combination antitumor therapy

Breast cancer is one of the most common invasive malignancies among women.[1] Although the early diagnosis and treatment of breast cancer have made significant progress in recent years, current treatment strategies and therapeutics still have unconquered limitations, especially for the triple negative breast cancer (TNBC). TNBC is a highly heterogeneous group of breast cancers that do not express or express low levels of estrogen receptor (ER), progesterone receptor (PR) and HER2/neu.[2] Notably, no effective standard therapy and proprietary drugs have been approved for TNBC treatment by the U.S. Food and Drug Administration (FDA), after initial responsiveness to chemotherapy and subsequent development of drug resistance.[3] Development of novel effective therapeutic strategies against TNBC is urgently needed.

Combination therapy, which targets and inhibits multiple essential pathways of tumor growth, invasiveness and/or metastasis, has great potential for enhancing therapeutic efficacy, lowering drug toxicity, and overcoming drug resistance, compared to monotherapy.[4−9] In recent years, strategies of combining photothermal therapy (PTT) or gene therapy with chemotherapy have been widely explored as potent antitumor approaches for those aggressive tumors with low overall survival rates.[10,11] Although it has been recognized that combination therapy is potentially effective for TNBC, only few successful investigations optimized for TNBC therapy with manageable dosing strategies have achieved enhanced therapeutic efficacy and manageable toxicity profile.[12−14]

Paclitaxel (PTX), a naturally occurring antimitotic agent, is an important agent in the chemotherapy of breast cancer.[15] However, the high hydrophobicity and serious side effects significantly limit its clinical application.[16] PTT has been extensively studied and shows satisfactory efficacy on primary and early stage metastatic breast cancer.[17] It has been documented that PTT can

* Address correspondence to niegj@nanoctr.cn, wuy@nanoctr.cn.

Received for review October 8, 2014 and accepted January 22, 2015.

Published online January 22, 2015
10.1021/nn505729m

selectively eliminate cancer stem cells in breast cancer.[18] Indocyanine green (ICG) has been approved by the FDA as a near-infrared (NIR) clinical imaging agent due to its remarkable optical features within the optimized window of *in vivo* applications, and has been used in PTT guided by its prominent photothermal conversion property with low long-term toxicity, in contrast to inorganic PTT agents.[19,20] However, ICG has intrinsic drawbacks, such as poor stability in aqueous solution and rapid blood clearance due to its inclined adhesion to plasma proteins.[21,22] Gene therapy, which can specifically target essential signaling pathways of cancer metabolic network, has shown great promise for treatment of breast cancer when combined with chemotherapy.[14] In the current study, we chose a small interfering RNA (siRNA) against survivin gene, which is critical for tumor cell survival.[23] The expression of survivin is closely related to the lymphatic metastasis of breast cancer which is the primary cause of TNBC's poor prognosis.[24] It has been demonstrated that survivin siRNA showed remarkably inhibition of tumor metastasis combined with chemotherapy and enhanced the sensitivity of tumor cells to chemotherapy.[25] To cope with the challenge of effective TNBC treatment, herein we present a strategy based on a tailor-designed "triple-punch" nanoplatform by integrating chemotherapy, gene therapy, and PTT into a combinatorial regimen. In this platform, an amphiphilic copolymer based nanocarrier was developed with the following advantages: (1) high payload and multidrug integration in a single nanostructure; (2) high biocompatibility and tumor targeting; (3) high responsiveness to tumor microenvironment and controlled drug release.

The amphiphilic nanocarrier was constructed by poly(2-(2-methoxyethoxy)ethyl methacrylate-*co*-oligo(ethylene glycol)methacrylate)-*co*-2-(dimethylamino)-ethyl methacrylate-*b*-poly(D,L-lactide-*co*-glycolide) (P (MEO_2MA-*co*-OEGMA-*co*-DMAEMA)-*b*-PLGA) (Figure 1A). The cationic polymer 2-(dimethylamino)ethyl methacrylate (PDMAEMA) offered positive charges to carry the negatively charged siRNA.[26,27] P (MEO_2MA-*co*-OEGMA) copolymer integrated the advantages of both polyethylene glycol (PEG) (low toxicity and anti-immunogenicity) and poly(*N*-isopropylacrylamide) (thermoresponsiveness).[28−30] The lower critical solution temperature (LCST) of P (MEO_2MA-*co*-OEGMA-*co*-DMAEMA)-*b*-PLGA can be modulated to slightly higher than body temperature by changing the ratios of MEO_2MA and OEGMA. Hydrophilic ICG and hydrophobic PTX were entrapped in the nanocarrier by an improved double emulsion method (Figure 1A).[31] Ideally, the thermoresponsiveness can ensure the stability of the core−shell nanoparticle (NP) and slow drug diffusion at a temperature below the LCST. Once the temperature is above the LCST, the hydrophilic component will rapidly collapse, resulting in the disassembly of the core−shell structure and triggering burst drug release.[32] Therefore, the selective PTX release from the nanocarrier can be triggered by the hyperthermia produced by ICG under NIR-laser irradiation.[33] The NP containing ICG, PTX and siRNA (NP-IPS) exhibited remarkable antitumor efficacy to TNBC due to the combinational effects of chemotherapy, photothermal therapy and gene therapy with low drug dose and minimal side effects (Figure 1B).

RESULT AND DISCUSSION

Fabrication and Characterization of NP-IPS. The synthesis procedure of P (MEO_2MA-*co*-OEGMA-*co*-DMAEMA)-*b*-PLGA was shown in Figure 1A. Hydroxyl-terminated P (MEO_2MA-*co*-OEGMA-*co*-DMAEMA) precursor copolymer was prepared by the radical copolymerization. Hydroxyethanethiol, the chain transfer agent (CTA), was used to introduce hydroxyl group to the end of the copolymer by telomerization. As listed in Supporting Information Tables S1 and S2, the average molecular weight (MW) and the LCST of the copolymers could be adjusted by changing the content of CTA or the ratios of MEO_2MA to OEGMA. An ideal LCST would be slightly higher than normal human body temperature so that a small temperature increase by local heating could induce the collapse of the micelles to trigger the release of encapsulated drug molecules. Therefore, hydroxyl-terminated P (MEO_2MA-*co*-OEGMA-*co*-DMAEMA) copolymer synthesized with the molar ratio of 95:5 (MEO_2MA:OEGMA) and the CTA content of 1.0% (mol %) was chosen in the following studies (LCST of 41.9 °C). P (MEO_2MA-*co*-OEGMA-*co*-DMAEMA)-*b*-PLGA block copolymers with various compositions and lengths of PLGA were synthesized by ring opening esterification polymerization. A typical ^1H NMR spectrum of copolymer C (Sample C in Supporting Information Table S3) was shown in Supporting Information Figure S1. Transmittance change of the NP composed of copolymer C in PBS buffer along with the change of temperature was shown in Supporting Information Figure S2. The characteristics of the copolymers were listed in Supporting Information Table S3. The critical micelle concentration (CMC) values of the copolymers ranged from 4.0 to 25.0 mg/L, indicating high stability of the NPs in aqueous solution (Supporting Information Table S4). An increased length of PLGA block yielded lower CMC. Copolymer C was finally chosen for the following study by considering the stability, particle size and polydispersity of the NPs.

The fabrication procedure of NP-IPS was shown in Figure 1A. The morphology of NP-IPS was characterized by transmission electron microscopy (TEM) and dynamic light scattering (DLS). NP-IPS was dispersed as individual particles with a typical spherical core−shell structure and a size of 100 nm (Figure 2A). When irradiated with an 808 nm laser at 1 W/cm^2

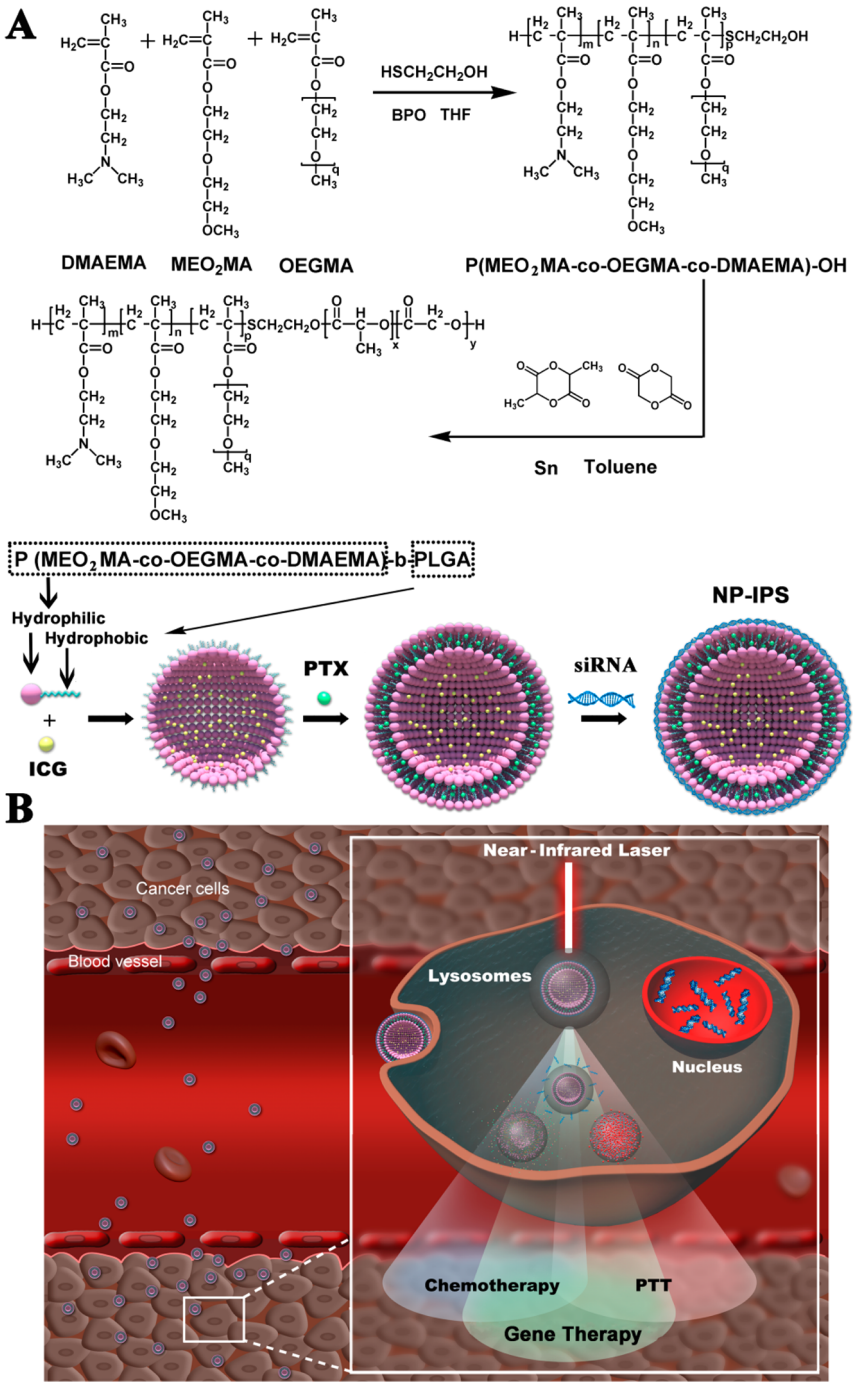

Figure 1. Schematic illustration of (A) synthesis route of P (MEO_2MA-*co*-OEGMA-*co*-DMAEMA)-*b*-PLGA and NP-IPS, and (B) the combination therapy to MDA-MB-231 tumors by NP-IPS.

for 5 min, the spherical core–shell structure of NP-IPS collapsed (Figure 2B), which was induced by the heat produced by ICG after NIR light irradiation at a temperature higher than the LCST of P (MEO_2MA-*co*-OEGMA-*co*-DMAEMA)-*b*-PLGA block copolymers.

We then investigated the sizes and surface charges of the different formations of NPs. After the NPs were loaded with multiple drugs, the sizes of such NPs increased slightly while their surface charges remained constant (Supporting Information Figure S3A,B). To evaluate the stability, NP-IPS was dissolved in PBS and stored at 37 °C for 3 days. As shown in Supporting Information Figure S3C,D, the sizes and the zeta potentials had no dramatic change. The effects of mass ratios of materials on encapsulation efficiency of ICG and PTX were shown in Supporting Information Table S5. And an optimal proportion of 20:1:1 (copolymer:ICG:PTX) was chosen for the subsequent studies.

The nucleic acid binding capability of NP was assessed using double stranded DNA (dsDNA) as the template by agarose gel electrophoresis assay,

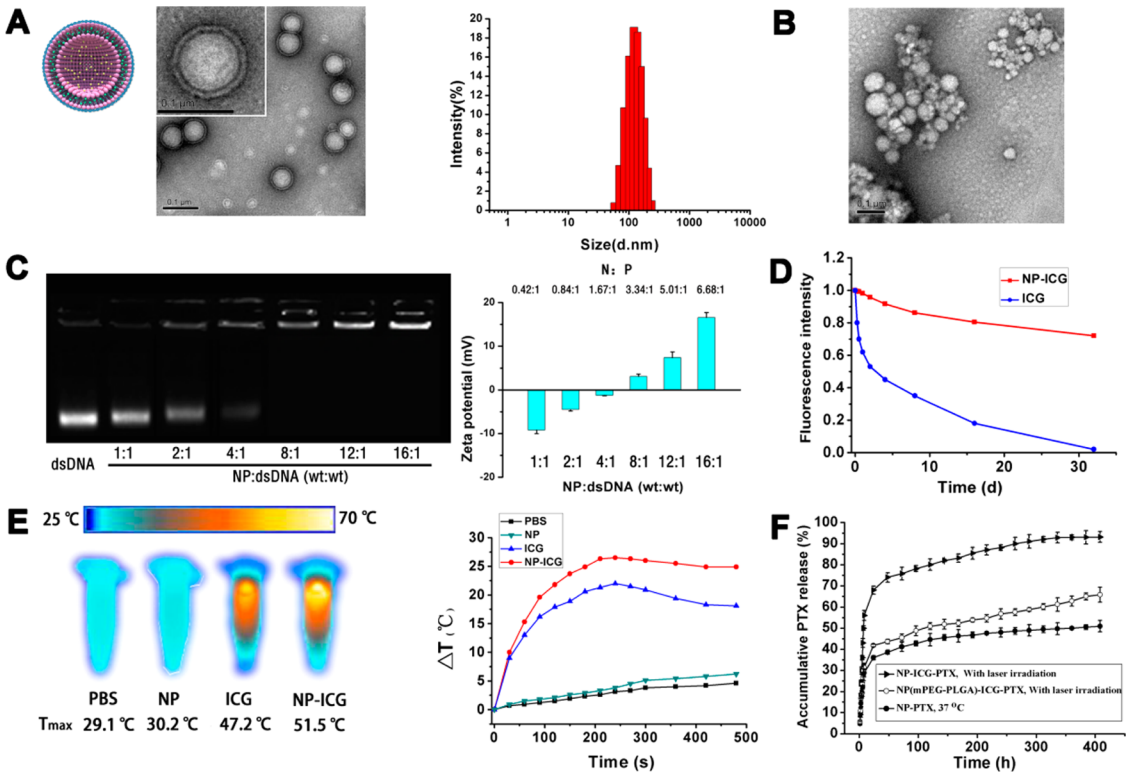

Figure 2. Characterization of the nanocarriers. (A) Characterization of NP-IPS by TEM and DLS. Scale bar, 0.1 μm. (B) TEM image of NP-IPS irradiated with an 808 nm laser at 1 W/cm^2 for 5 min. Scale bar, 0.1 μm. (C) Electrophoretic mobility and zeta potential changes of NPs after loading with different amounts of dsDNA. N:P, nitrogen-to-phosphorus ratio of NP-dsDNA. (D) Fluorescence stability of NP-ICG and ICG. (E) The infrared thermal image and maximum temperature profiles of NP-ICG, ICG, NP, and PBS under continuous laser irradiation (1 W/cm^2) for 8 min. (F) PTX release profiles of NP-ICG-PTX and NP (mPEG−PLGA)-ICG-PTX at 37 °C or with laser irradiation (1 W/cm^2) for 5 min.

at the ratios of NP/dsDNA (w/w) ranging from 1:1 to 16:1. The mobility of dsDNA was completely retarded by the NPs at the ratio higher than 1:4. Coating with dsDNA can reverse the surface charges of NPs. When the ratios varied from 16:1 to 1:1, the zeta potentials changed from +17.4 to −9.8 mV (Figure 2C). These results indicated that NP had a large capacity to bind negatively charged nucleic acids. Moreover, the negative charged siRNA attached to the surface of positive charged NPs *via* electrostatic interaction was protected from degradation in serum-containing medium (Supporting Information Figure S4).

To investigate whether NP-ICG had a higher stability than ICG, absorption spectra of ICG and NP-ICG were measured after storage in dark at room temperature for different time intervals. NP-ICG exhibited a slight reduction of the absorbance after 30 days (Supporting Information Figure S5A), while ICG almost completely degraded (Supporting Information Figure S5B). Analogously, fluorescence intensity of NP-ICG reduced a little, while that of ICG completely disappeared after 30 days (Figure 2D). These data demonstrate that the stability of ICG was significantly increased after encapsulated by the NP. Because ICG exhibits much higher photostability in high concentration (aggregated form) than in low concentration of aqueous solution, the photoprotection may be derived from the greatly increased local concentration of loaded-ICG facilitated by the NP.[34]

To assess the photothermal efficiency of NP-ICG, we detected the change of temperature using an infrared thermal imaging camera under laser irradiation *in vitro*. With the laser irradiation at 1 W/cm^2 for 8 min, the temperatures of NP-ICG and ICG groups increased to 51.5 and 47.2 °C, respectively, which can lead to an irreversible damage to tumor cells, while the temperatures of PBS and the NP groups only increased to 29.1 and 30.2 °C (Figure 2E).[17] Our results showed that NP-ICG possesses higher photothermal efficiency than free ICG, most likely because of the improved photostability of encapsulated-ICG in aqueous solution derived from the NP encapsulation.

In vitro PTX release from the NPs was studied in PBS at 37 °C (below the LCST of the NP) or after the laser irradiation (the temperature above the LCST of the NP). To evaluate the controlled release profile of PTX, the nonthermosensitive polymer mPEG−PLGA nanoparticles (NP (mPEG−PLGA)) was served as a control. As shown in Figure 2F, at 37 °C, PTX was released from the NP with an initial burst (reaching 30% within the first 8 h) followed by a continuously slow release phase. Under laser irradiation, PTX release from the NP was

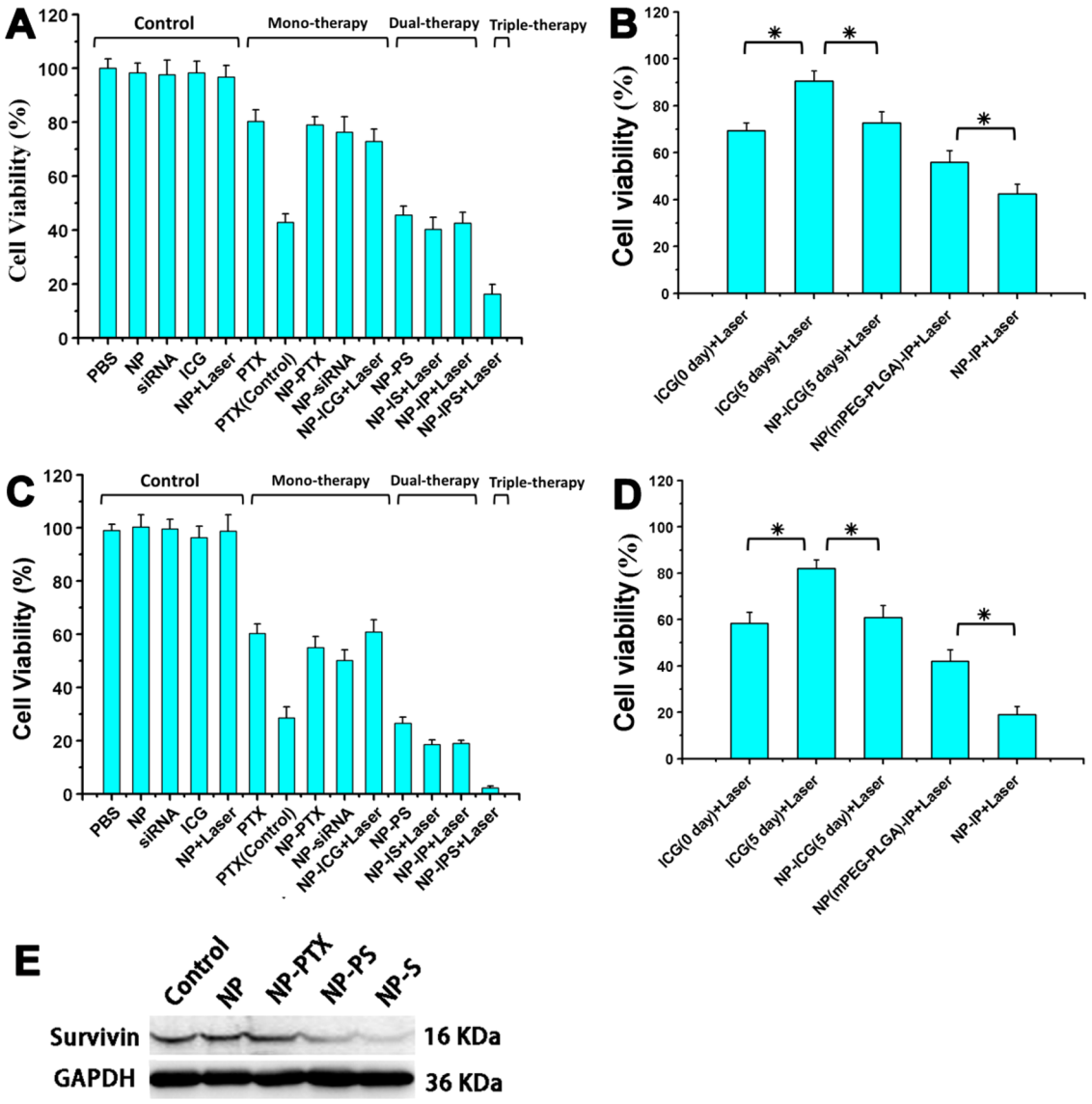

Figure 3. ***In vitro*** **antitumor activity against MDA-MB-231 cells. Cell viability of MDA-MB-231 cells treated with different forms of NPs with or without laser irradiation at 37 °C for 24 h (A and B) or 48 h (C and D). PTX, 0.1 μg/mL; PTX (control), 10 μg/mL. *$p < 0.05$. (E) Western blot analysis of the expression of survivin protein in MDA-MB-231 human breast cancer cells after treatment with different formulations for 48 h.**

much faster. Within the first 8 h, more than 60% PTX was released, while PTX release from nonthermoresponsive NP(mPEG−PLGA) with laser irradiation was similar to that from the NP at 37 °C. These results demonstrated that NP can achieve controlled and efficient drug release by laser irradiation. When the temperature was below the LCST, the core−shell structure of NP was stable and the diffusion of PTX was slow. However, once the temperature was increased above the LCST by laser irradiation, the hydrophilic component collapsed which induced the deformation of the whole core−shell structure and accelerated drug release.

In Vitro **Antitumor Activity of NP-IPS against MDA-MB-231 Cells.** To investigate the combinational effects of the codelivered PTT agent (ICG), chemotherapeutic drug (PTX) and gene therapy agent (a validated survivin siRNA, GAA UUA ACC CUU GGU GAA UTT), MDA-MB-231 human breast cancer cells were treated with different drug formulations for 24 or 48 h, followed by quantification of cell viability. Schematic illustration of the proposed process of combination therapy to MDA-MB-231 cells by NP-IPS was shown in Figure 1B. The results showed that all drug formulations led to decreased cell viability after 24 h (Figure 3A,B) or 48 h (Figure 3C,D) treatment, while the control groups (PBS, NP, siRNA, ICG and NP + Laser) had almost no effect on cell viability. The monotherapy groups only slightly decreased cell viability because the current drug doses (final concentrations: ICG, 0.1 μg/mL; PTX, 0.1 μg/mL; survivin siRNA, 100 nM) were much lower than their effective concentrations. In the current study, 50% inhibitive concentration of PTX within 24 h is about

10 μg/mL, which is 100 times more than the concentration of encapsulated PTX (Figure 3A,C). Triple-therapy group exhibited a remarkably combinational effect than the dual-therapy groups. These results indicated that NP-IPS coupled with laser irradiation could produce the highest cytotoxicity, which confirmed our anticipation that combinational efficacy would be achieved when integrating PTX, ICG, and survivin siRNA into a single nanoplatform. Since NP-ICG has higher stability than free ICG, ICG (fresh prepared) and NP-ICG (stored in dark for 5 days) had increased cytotoxicity compared to free ICG (stored in dark for 5 days) under laser irradiation, suggesting enhanced PTT efficiency of ICG by NP formulation (Figure 2C). NP-IP coupled with laser radiation group showed much higher cytotoxicity than NP (mPEG−PLGA)-IP, demonstrating thermoresponsive burst drug release contributed to the enhanced therapeutic efficiency of the sensitive NPs (Figure 3B,D).

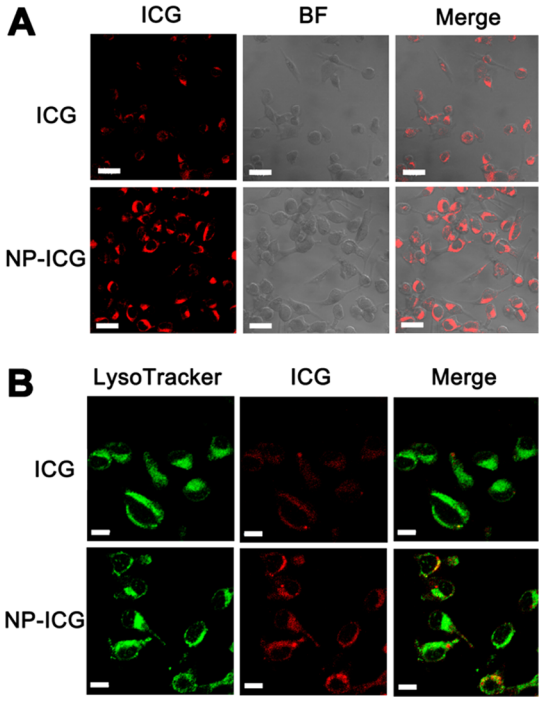

Figure 4. *In vitro* **imaging. (A)** *In vitro* **fluorescence images of MDA-MB-231 cells after labeling with ICG and NP-ICG (BF, bright field). Scale bars, 30 μm. (B) The fluorescence images of MDA-MB-231 cells labeled with ICG, NP-ICG and LysoTracker. Scale bars, 10 μm.**

The cellular survivin gene silencing efficiencies of different formulations were evaluated by Western blot analysis. The expression of survivin protein was dramatically down-regulated by NP-PS and NP-siRNA, but not the null NP (Figure 3E), confirming the intracellular delivery efficiency of survivin siRNA by our nanocarrier.

Endocytosis and Subcellular Localization of the NPs. We next studied the endocytosis and subcellular localization of the NPs by confocal microscopy. Significantly stronger fluorescent signals were observed in MDA-MB-231 cells treated with NP-ICG compared to those treated with free ICG, indicating enhanced internalization and/or stability of ICG by NP formulation (Figure 4A). Moreover, the majority of NP-ICG was found to be localized in lysosomal acidic compartment (Figure 4B).

***In Vivo* Distribution of the NPs.** To investigate the *in vivo* distribution of the NPs, nude mice were intravenously injected with saline, ICG or NP-ICG. Ventral

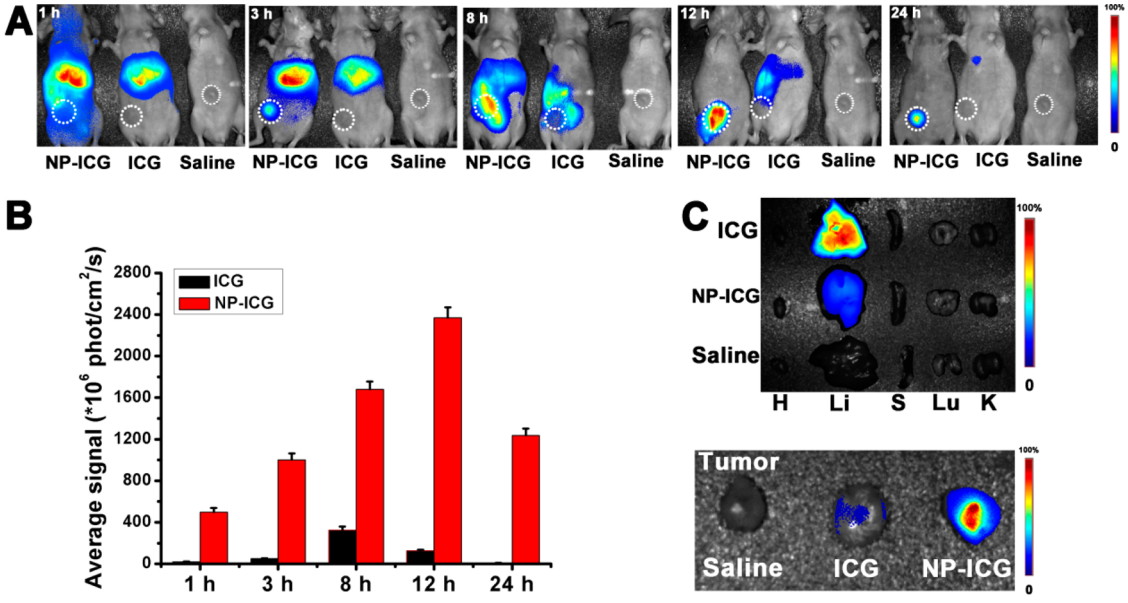

Figure 5. *In vivo* **and** *ex vivo* **imaging. (A)** *In vivo* **fluorescence images of BALB/c nude mice 1, 3, 8, 12, and 24 h after administration of saline, ICG or NP-ICG. (B) Average fluorescence signals of tumors 1, 3, 8, 12, and 24 h after administration of ICG and NP-ICG. (C)** *Ex vivo* **fluorescence images of major organs and tumors 24 h after administration of saline, ICG, or NP-ICG (H, heart; Li, liver; S, spleen; Lu, lung; K, kidney).**

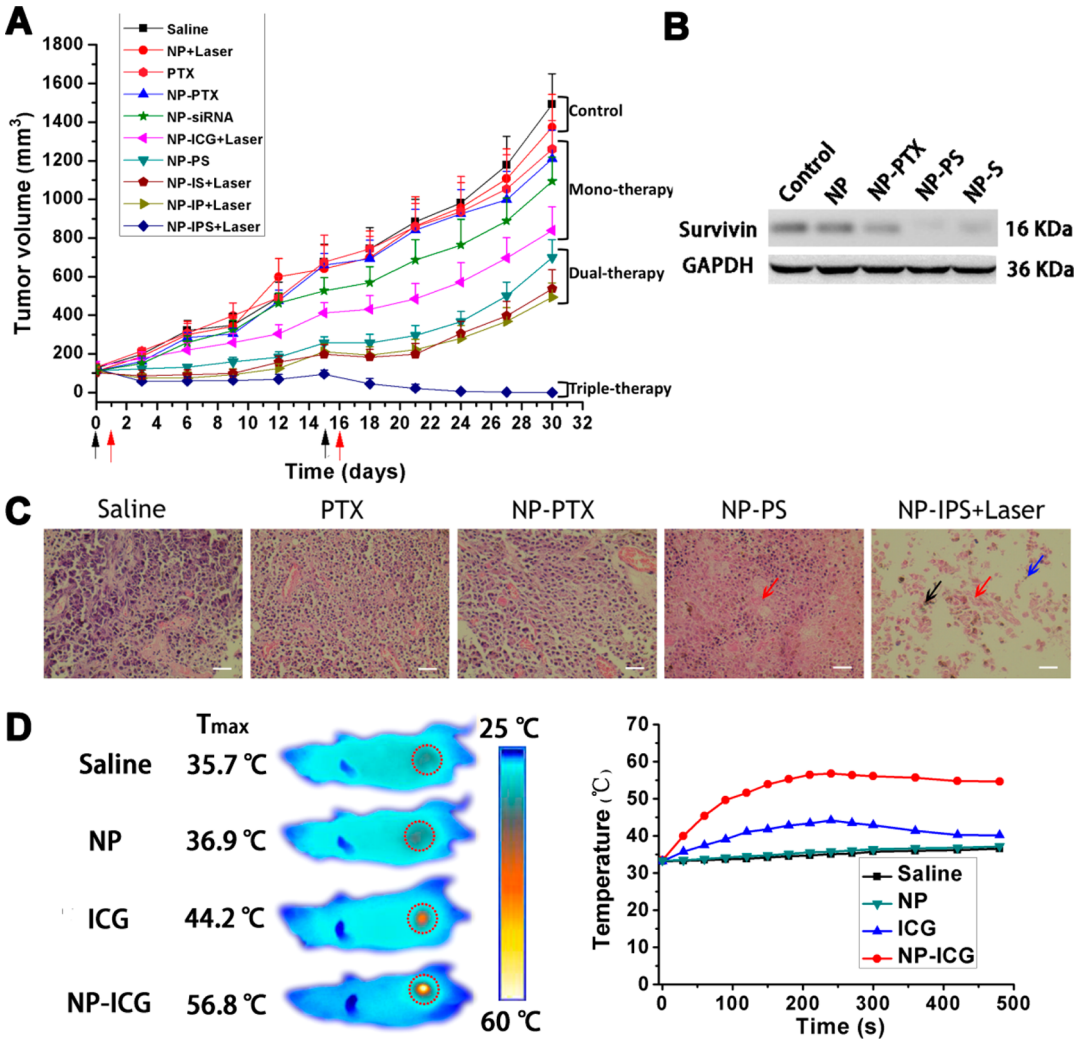

Figure 6. *In vivo* **antitumor activity of NPs. (A) Antitumor activities of various drug formulations in a xenograft model of human breast cancer in BALB/c athymic nude mice. Mice bearing MDA-MB-231 tumors (~0.1 cm^3) were treated with different reagents (n = 5). The treatment schedule was indicated by black arrows for intravenous injection and red arrows for the laser irradiation. (B) The expression of survivin in tumor tissues detected by Western blot 2 days after the second injection. (C) Representative H&E sections of tumors after treatment with saline, PTX, NP-PTX, NP-PS, or NP-IPS + Laser. Red arrow, karyolysis; blue arrow, abundant pykonosis; black arrow, coagulative necrosis. The tissue sections were 5 μm thick. Scale bars, 50 μm. (D) Infrared thermographic maps of tumors after laser irradiation for 8 min and maximum temperature profiles of the irradiated tumor areas of nude mice treated with NP-ICG, ICG, NP, or saline.**

fluorescence signals were captured at 1, 3, 8, 12, and 24 h after injection using a Maestro *in vivo* optical imaging system. As shown in Figure 5A,B, strong ICG fluorescence was observed in the whole liver area in NP-ICG group 1 h after the injection, similar to that of ICG group. Along with the increase in circulation time, stronger signals appeared at the tumor site in NP-ICG group, while signals of ICG group were mainly located around the liver. In contrast to free ICG, NP-ICG possesses excellent passive tumor targeting ability, evidenced by the highest signal intensity in tumor 12 h postinjection and complete NP clearance from the body 24 h postinjection. The *ex vivo* fluorescent images of excised tissues further confirmed much higher accumulation of NP-ICG compared to free ICG in tumors (Figure 5C). No obvious fluorescence signals were observed in the heart, spleen, lung and kidney in NP-ICG group, while a dramatic accumulation of ICG was located in the liver in free ICG group (Figure 5C). These results demonstrated that NP-ICG could significantly accumulate in tumor region by the enhanced passive targeting effect in the animal model.[30]

***In Vivo* Antitumor Activity of NPs.** We next investigated the therapeutic effects of the NP *in vivo*. As shown in Figure 6A and Supporting Information Figure S6, fast tumor growth curves were obtained in the control groups (saline and null NP coupled with laser), suggesting that the MDA-MB-231 tumor growth was not affected by null NP and/or laser irradiation. The growth of MDA-MB-231 tumors were slightly inhibited by monotherapy groups because of the low drug dosage used (ICG, 0.32 μmol/kg; PTX, 0.54 μmol/kg; siRNA, 1.5 mg/kg). For the dual-therapy groups, the tumors were inhibited remarkably at the beginning, but tumor

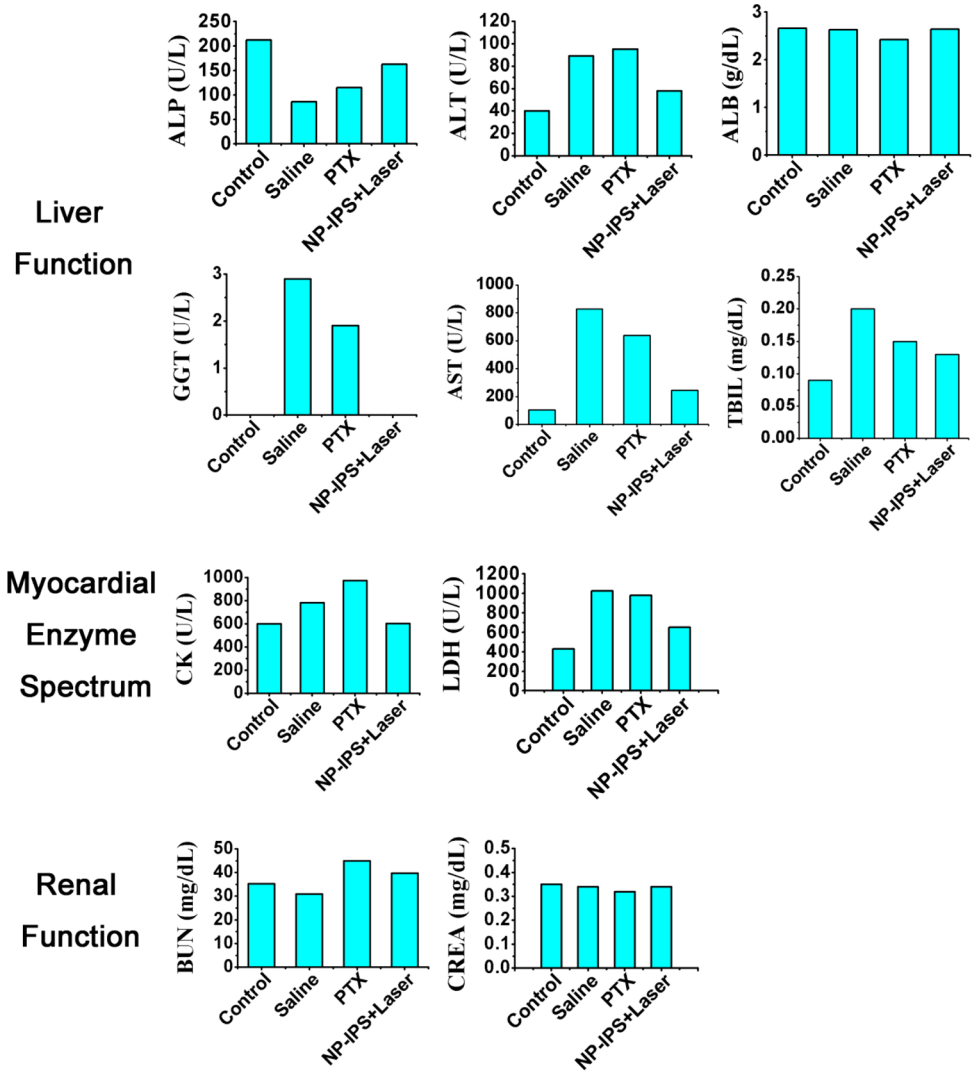

Figure 7. Serum biochemical examination of NP-IPS-treated mice. Normal BALB/c nude mice served as control group. Data were presented as mean ± SD (n = 5). ALB, Albumin; AST, aspartate transaminase; ALT, alanine aminotransferase; ALP, alkaline phosphatase; GGT, gamma glutamyl transpeptidase; TBIL, total bilirubin; LDH, lactate dehydrogenase; CK, creatine kinase; CREA, creatinine; BUN, blood urea nitrogen.

recurrence happened rapidly. Notably, the triple-therapy group represented the best therapeutic effect, showing complete growth inhibition and remission without tumor recurrence. These results demonstrated that our nanoplatform can achieve combinational antitumor effects with minimized individual drug dosage.

To examine the delivery efficiency of survivin siRNA by our nanocarrier *in vivo*, expression of survivin protein in tumor tissues was evaluated by Western blot after treatment with NPs in different formulations. As shown in Figure 6B, the expression of survivin protein in tumor tissue was significantly down-regulated when treated with NP-PS and NP-S compared to the other control groups. These results demonstrated that our nanocarrier effectively delivered survivin siRNA into tumor tissues.

To further examine the antitumor effect of various drug formulations *in vivo*, we studied the histopathology of the tumor tissue after treatments with various drug formulations (Figure 6C). Tumors treated with saline, PTX and NP-PTX alone showed no obvious damage due to the low drug dose. However, tumors treated with NP-PS revealed regions of karyolysis (red arrow in Figure 6C) and NP-IPS coupled with laser group exhibited more considerable regions of karyolysis. In addition, typical thermal damage features (abundant pykonosis, blue arrow in Figure 6C; coagulative necrosis, black arrow in Figure 6C) were observed in NP-IPS coupled with laser group.[17]

To assess the photothermal efficiency of NP-ICG *in vivo*, we detected the changes of tumor temperature using an infrared thermal imaging camera under laser irradiation *in vivo* (Figure 6D). With the laser irradiation at 1 W/cm^2 for 5 min, the maximum temperatures of the tumors treated with NP-ICG reached 56.8 °C which can lead to an irreversible damage to tumor cells, while

the local temperature in the tumors treated with free ICG alone increased to 44.2 °C at most.[17] However, the saline and null NPs treated tumors under the same laser irradiation resulted in a temperature increase to 35.7 and 36.9 °C, which cannot damage the tumor irreversibly.

***In Vivo* Potential Effects of NPs.** To examine any potential damage to major organs after treatments with various drug formulations in tumor-bearing mice, we studied the post-mortem histopathology of the heart, liver, spleen, lung and kidney in all groups. As shown in Supporting Information Figure S7, no obvious morphological differences were observed among these groups. To further illustrate the efficacy of these treatments, we measured serum biochemical indices. Significant differences of the biochemical indicators in the liver, heart and kidney were observed between the tumor-bearing mice and the normal nude mice (control), which were mainly due to the implantation of tumor xenografts (Figure 7). After treatment with NP-IPS coupled with laser, the organ functions, revealed by biochemical indicators, tended to the normal levels, in accordance with the inhibition of tumor growth. No additional serum biochemical abnormality was observed when treated with various NP formulations.

CONCLUSIONS

In conclusion, we successfully designed and fabricated the well-defined NP-IPS based on a thermosensitive amphiphilic copolymer, which simultaneously delivered ICG, PTX and siRNA to tumor regions for triple-therapy against TNBC. The NP-IPS significantly enhanced the stability of ICG and realized controlled release of the PTX in tumor regions, which was triggered by the hyperthermia produced by near-infrared laser irradiated ICG. NP-IPS demonstrated remarkable antitumor efficacy against TNBC, due to the combinational effects of chemotherapy, PTT and gene therapy. Meanwhile, the individual drug dosage was minimized and no obvious toxic effect on the major organs was observed. Therefore, the triple-punch strategy by NP-IPS plus laser could be a promising strategy for further development as a mainstream strategy for TNBC treatment.

MATERIALS AND METHODS

Materials. 2-(2-Methoxyethoxy)ethyl methacrylate, oligo(ethylene glycol)methacrylate, 2-(dimethylamino)ethyl methacrylate, D,L-lactide (LA), glycolide (GA), pyrene, 2-hydroxyethanethiol, tin(II)2-ethylhexanoate, benzoyl peroxide (BPO) and indocyanine green (ICG) were purchased from Sigma-Aldrich (St. Louis, MO). Paclitaxel (PTX) was purchased from Beijing HuaFeng Unite Co., Ltd. (Beijing, China). Phosphate-buffered saline (PBS, pH 7.4) was purchased from Beijing Leagene Biotechnology Co., Ltd. (Beijing, China). Cell counting kit-8 was purchased from Dojindo Molecular Technologies (Tokyo, Japan). Dulbecco's modified Eagle's medium (DMEM) and fetal bovine serum were purchased from Gibco BRL (Grand Island, NY). Penicillin and streptomycin were provided by Sigma-Aldrich (St. Louis, MO). LysoTracker Green DND-26 was purchased from Molecular Probes (Eugene, OR). Survivin siRNA was obtained from RiboBio Co., Ltd. (Guangzhou, China). Anti-survivin antibody and goat anti-rabbit IgG (H+L) HRP were purchased from Bioworld Technology, Co., Ltd. (Nanjing, China).

Synthesis of P (MEO_2MA-*co*-OEGMA-*co*-DMAEMA)-*b*-PLGA). Briefly, hydroxyl-terminated poly(2-(2-methoxyethoxy)ethyl methacrylate-*co*-oligo(ethylene glycol) methacrylate-*co*-2-(dimethylamino) ethyl methacrylate) precursor copolymer was prepared by the radical copolymerization using 2-hydroxyethanethiol as a chain transfer agent (CTA) and benzoyl peroxide (BPO) as an initiator. For instance, 2-(2-methoxyethoxy)ethyl methacrylate (162.32 mmol), oligo(ethylene glycol) methacrylate (18.02 mmol), 2-(dimethylamino)ethyl methacrylate (17.69 mmol), 2-hydroxyethanethiol (2.21 mmol) and BPO (0.29 mmol) were dissolved in 30 mL of THF. The reaction mixture was refluxed at 70 °C for 7 h under nitrogen after it was degassed by nitrogen for 20 min. Then, diethyl ether was added to precipitate the product. A slow liquid−liquid diffusion method was used to purify the products by reprecipitation twice from dichloromethane-diethyl ether. P (MEO_2MA-*co*-OEGMA-*co*-DMAEMA)-*b*-PLGA was synthesized by the ring-opening esterification polymerization of the hydroxy-terminated precursor with glycolide (GA) and D,L-lactide (LA) using $Sn(Oct)_2$ as the catalyst in toluene. The reaction mixture was refluxed at 120 °C for 24 h under nitrogen atmosphere.

Characterization of P (MEO_2MA-*co*-OEGMA-*co*-DMAEMA)-*b*-PLGA. The copolymers' molecular weights (MW) were detected by a gel-permeation chromatography (GPC) (Waters 2410, Milford, MA). The mobile phase was THF and the flow rate was 1 mL/min. The chemical structure of P (MEO_2MA-*co*-OEGMA-*co*-DMAEMA)-*b*-PLGA was confirmed by nuclear magnetic resonance (NMR) spectral analysis. ^{1}H NMR spectra of the copolymer were acquired by a Bruker AVANCE 400 NMR spectrometer (Billerica, MA). Optical transmittance of the copolymer solution (5 mg/mL) was detected with a UV−vis spectrometer (UV-2501PC, Shimadzu, Japan) at 500 nm. A temperature-controller (TCC-240A, Shimadzu, Japan) was used to control the temperature of the sample cells. The temperatures showing an optical transmittance of 50% were the LCST values of copolymer solutions.

The critical micelle concentration (CMC) of the copolymer in deionized water and PBS (pH 7.4) was detected by fluorescence spectroscopy using pyrene as a probe. Fluorescence spectra were acquired by a LS 55 Fluorescence Spectrometer (PerkinElmer, Fremont, CA) at 25 °C. Pyrene dissolved in acetone (4.8×10^{-4} M, 5 μL) was added to 4 mL of copolymer solutions in a series of concentrations. The final concentration of pyrene was 6.16×10^{-7} M. The solutions were kept for 24 h at 25 °C. The recorded excitation spectra were of 340 nm with an emission wavelength of 370−400 nm. Both excitation and emission bandwidths were set at 5 nm. The intensity ratios (I_1/I_3) were plotted as a function of copolymer concentration's logarithm. The CMC value was drawn from the crossing point of the tangent to the curve with the horizontal tangent through the points.

Preparations of P (MEO_2MA-*co*-OEGMA-*co*-DMAEMA)-*b*-PLGA Nanoparticle (NP), NP-ICG, NP-PTX, NP-ICG-PTX (NP-IP), and NP-ICG-PTX-siRNA (NP-IPS). NP-IP was prepared by the improved double emulsion (W/O/W) method. Briefly, 20 mg of P (MEO_2MA-*co*-OEGMA-*co*-DMAEMA)-*b*-PLGA dissolved in 1 mL of methylene chloride and 0.2 mL of ICG aqueous solution was transferred to a centrifuge tube, and the mixture was emulsified by sonication for 3 min. Then 2 mL of 2% poly(vinyl alcohol) (PVA) was added into the mixture and the solution stirred for 3 min. Meanwhile, 0.2 mL PTX dissolved in methylene chloride was added slowly, and then emulsified by sonication for 8 min. The mixture was then slowly added into 10 mL of 0.3% PVA and stirred for 10 min. After evaporation under reduced pressure, the NP was precipitated by centrifugation at 13 000 rpm for 10 min and washed

with deionized water three times. The same procedures were used to prepare the NP, NP-ICG, and NP-PTX in the absence of PTX or ICG. For the preparation of NP-IPS, 20 μg of siRNA was dissolved in 100 μL nuclease-free water and the solution was added to 1 mL of NP-IP nuclease-free water solution. Then the mixture was incubated for 30 min at 25 °C.

Characterization of the NPs. The average size, zeta potential and polydispersity index were detected by dynamic light scattering (DLS) using a ZetaSizer Nano series Nano-ZS (Malvern Instruments Ltd., Malvern, U.K.). Detections were at 633 nm with a constant angle of 90° at 25 °C after samples were appropriately diluted in PBS. The morphology of the NP-IPS with or without laser irradiation was determined by transmission electron microscopy (TEM) (EM-200CX; JEOL Ltd., Tokyo, Japan) after negative staining with uranyl acetate.

The loading content (LC) and encapsulation efficiency (EE) of ICG were detected by LS 55 Fluorescence Spectrometer (PerkinElmer, Fremont, CA) with emission at 820 nm and excitation at 735 nm. The LC and EE of PTX were detected by HPLC (Waters 2478, Milford, MA) with UV detection at 227 nm. A C18-column (Nova-Pak 3.9 × 250 mm, Waters, Milford, MA) was used with a mobile phase composed of water and acetonitrile (20:80, v/v) and the flow rate of 1 mL/min. The LC and EE were defined as following formula: LC = (weight of loaded drug)/(total weight of NP and drug) × 100%; EE = (weight of loaded drug)/(weight of initially added drug) × 100%.

In vitro release of PTX from NP was detected by dialysis method. The freeze-dried NP-ICG-PTX was dispersed in 3 mL PBS and then introduced into a dialysis bag (molecular weight cutoff: 3500 Da). The end-sealed dialysis bag was incubated in 30 mL PBS at 37 °C with or without 808 nm continuous-wave diode laser (Daheng Science & Technology, China) irradiation at 1 W/cm^2 for 5 min (diameter of the laser spots, 4 mm) and shaken at a speed of 100 rpm using a water-bathing constant temperature vibrator. One milliliter of supernatant was taken at predetermined time intervals and replaced with 1 mL fresh PBS. The concentration of PTX released from NPs was detected by HPLC as described above. The PTX release from mPEG−PLGA NP was used as the control group.

The absorption spectra of ICG and NP-ICG were obtained by UV−vis spectrometer (UV-2501PC, Shimadzu, Japan). Fluorescence spectra were obtained by LS 55 Fluorescence Spectrometer (PerkinElmer, Fremont, CA) with excitation at 735 nm to monitor ICG. Fluorescent intensity at 820 nm of ICG and NP-ICG at predetermined times was measured in deionized water.

Agarose gel electrophoresis was performed to assess nucleic acid loading ability of the NPs. The NP-dsDNA complexes with different NP/dsDNA (w/w) ratios ranging from 1 to 16 were prepared. In detail, dsDNA was diluted in 10 mM HEPES (pH = 7.3) at the final concentration of 1 mg/50 mL. Complexes were prepared by adding plasmid solution (containing 1 mg DNA) to NPs solution at various NP/dsDNA (w/w) ratios by pipetting and incubated for 30 min. Four milliliters of 6× loading buffer was added into 20 mL of the NP-dsDNA (0.2 mg) complexes solution, and the mixture was loaded into a 0.8 wt % agarose gel (0.5 mg/mL ethidium bromide). Electrophoresis was in 1× TAE buffer at 120 V and run for 40 min. DNA was analyzed on UV illuminator to show its location.

***In Vitro* Cellular Uptake.** MDA-MB-231 cells were seeded onto a borosilicate chambered cover glass at a density of 2 × 10^5 cells per well at 37 °C for 24 h. Then, the medium was replaced by the medium containing ICG or NP-ICG. After incubation at 37 °C for 4 h, the cells were washed with PBS 3 times. Then the cells were imaged using an UltraVIEW Vox spinning disc confocal microscope (PerkinElmer Inc.).

For intracellular location of the NPs, MDA-MB-231 cells were seeded onto a borosilicate chambered cover glass at a density of 2 × 10^5 cells per well at 37 °C for 24 h. Then, the medium was replaced by the medium containing ICG or NP-ICG. After incubation at 37 °C for 4 h, the cells were washed with PBS 3 times. Then cellular acidic organelles were labeled by LysoTracker Green DND-26. After 30 min incubation at 37 °C, the cells were washed with PBS 3 times before image acquisition and observed at 60× magnification using UltraVIEW Vox confocal imaging system (PerkinElmer, Fremont, CA).

Cytotoxicity Assay. MDA-MB-231 cells were seeded in 96-well plates at a density of 2 × 10^4 cells per well and incubated at 37 °C with 5% CO_2 for 12 h. The culture media were removed and then replaced by 200 μL of DMEM supplemented with 10% fetal bovine serum containing equivalent concentrations of PBS, NP, PTX, siRNA, ICG, NP-PTX, NP-siRNA, NP-IP, NP-IPS (final ICG concentration 0.1 μg/mL, final PTX concentration 0.1 μg/mL, final siRNA concentration 100 nM) for 24 or 48 h, respectively. Then the viability of cells was detected by a CCK-8 assay. To investigate the PTT efficacy, MDA-MB-231 cells were seeded at a density of 2 × 10^4 cells per well in 96-well plates and incubated at 37 °C with 5% CO_2 for 12 h before evaluation. The culture media were removed and then replaced by 200 μL of DMEM supplemented with 10% fetal bovine serum containing equivalent concentrations of NP, ICG (fresh), ICG (5 days), NP-ICG (5 days), NP (mPEG−PLGA)-IP, NP-IS, NP-IP, NP-IPS (final ICG concentration, 0.1 μg/mL; final PTX concentration, 0.1 μg/mL; final siRNA concentration, 100 nM). After 24 h incubation, the cells were irradiated with a 1 W/cm^2 808 nm laser for 5 min (diameter of the laser spots, 4 mm). After another 12 or 36 h incubation, the viability of cells was detected by a CCK-8 assay.

Western Blot Analysis. Total proteins were harvested from treated MDA-MB-231 human breast cancer cells and analyzed by Western blot after treatment with different formulations. Proteins harvested from MDA-MB-231 implanted tumor tissues after treatment with different formulations were also analyzed by Western blot.

Animals and Tumor Model. Female BALB/c athymic nude mice, 6−7 weeks of age weighting 18−23 g, were purchased from Beijing Vital River Laboratories. MDA-MB-231 human breast cancer cells (2.0 × 10^6 cells in 50 μL PBS) mixed with 50 μL of matrigel were transplanted into the mammary fat pads of the mice, and allowed to grow to a tumor size ~0.1 cm^3 (volume = length × width^2/2, measured with a vernier caliper). The mice were then randomly divided into different experimental groups (5 mice/group) as described in the Results and Discussion section. All procedures were approved by the Committee on the Ethics of Animal Experiments of the Health Science Center of Peking University (Beijing, China).

Temperature Measurements during Laser Irradiation. PBS (500 μL), NP (500 μL), ICG (500 μL, containing 25 μg/mL ICG), and NP-ICG (500 μL, containing 25 μg/mL ICG) were added to centrifuge tubes. The nude mice bearing MDA-MB-231 tumors were injected with 150 μL of saline, NP, ICG (containing 25 μg/mL ICG) or NP-ICG (containing 25 μg/mL ICG) through the tail vein. The tubes and tumors were irradiated by the 808 nm laser at 1 W/cm^2 for 8 min (diameter of the laser spots, 8 mm). Region maximum temperatures and infrared thermographic maps were obtained with an infrared thermal imaging camera (Ti27, Fluke).

***In Vivo* Imaging and Biodistribution Analysis.** *In vivo* fluorescent images of nude mice were taken using the *ex/in vivo* imaging system (CRi, Woburn, MA) with a 704 nm excitation wavelength and a 735 nm filter to collect the FL signals of ICG 1, 3, 8, 12, and 24 h after tail vein injection with 150 μL of saline, 150 μL of ICG (0.32 μmol/kg, ICG) or 150 μL of NP-ICG (0.32 μmol/kg, ICG). The mice after *in vivo* imaging were sacrificed and the tumors, hearts, livers, spleens, lungs, kidneys were collected for imaging.

***In Vivo* Treatments.** The mice were injected though the tail vein with 150 μL of saline, NP, PTX (0.54 μmol/kg), NP-PTX (PTX, 0.54 μmol/kg), NP-siRNA (siRNA, 1.5 mg/kg), NP-PS (PTX, 0.54 μmol/kg; siRNA, 1.5 mg/kg), NP-ICG (ICG, 0.32 μmol/kg), NP-IP (ICG, 0.32 μmol/kg; PTX, 0.54 μmol/kg), NP-IS (ICG, 0.32 μmol/kg; siRNA, 1.5 mg/kg) or NP-IPS (ICG, 0.32 μmol/kg; PTX, 0.54 μmol/kg; siRNA, 1.5 mg/kg). For the laser treatment groups, the tumors of mice were irradiated by the 808 nm laser at 1 W/cm^2 for 5 min (diameter of the laser spots, 8 mm) The tumor volumes of each mouse were measured with a vernier caliper.

Evaluations of Potential Side Effects Associated with Drug Administration. Tumor-bearing athymic nude mice (n = 5) were intravenously injected with saline, PTX (0.54 μmol/kg), NP-PTX (PTX, 0.54 μmol/kg), NP-PS (PTX, 0.54 μmol/kg; siRNA, 1.5 mg/kg) or NP-IPS (ICG, 0.32 μmol/kg; PTX, 0.54 μmol/kg; siRNA, 1.5 mg/kg) on days 1 and 5. The mice in NP-IPS group received laser

treatment on days 2 and 6. On day 7, mice were sacrificed and sera were collected for biochemical studies (Clinical Laboratory). Serial sections of formalin-fixed tumors as well as various organs embedded in paraffin were stained with hematoxylin and eosin (H&E) and analyzed at 40× magnification (boxed region is amplified eight times in the bottom panels).

Conflict of Interest: The authors declare no competing financial interest.

Acknowledgment. This work was supported by grants from MoST 973 programs (2012CB934000 and 2010CB934004), the NSFC programs (31325010, 81272453 and 31300822).

Supporting Information Available: Properties of the precursor copolymers and the block copolymers; effects of mass ratio of materials on encapsulation efficiency and loading content; ^{1}H NMR spectrum of P (MEO_2MA-*co*-OEGMA-*co*-DMAEMA)-*b*-PLGA in $CDCl_3$; transmittance change of NPs in PBS as a function of temperature; particle sizes and zeta potentials of different forms of NPs and the stability of NP-IPS; the stability of free and nanoparticle carried siRNA in DMEM medium (10% FBS) at 37 °C; absorption spectra of NP-ICG and ICG after different storage times; the statistical comparison of the tumor growth in mice after various treatments on day 30; representative H&E sections of various organs of tumor-bearing BALB/c mice after treatment with saline, PTX, NP-PTX, NP-PS, or NP-IPS + Laser. This material is available free of charge *via* the Internet at http://pubs.acs.org.

REFERENCES AND NOTES

1. Kamangar, F.; Dores, G. M.; Anderson, W. F. Patterns of Cancer Incidence, Mortality, and Prevalence across Five Continents: Defining Priorities To Reduce Cancer Disparities in Different Geographic Regions of the World. *J. Clin. Oncol.* **2006**, *24*, 2137–2150.
2. Carey, L.; Winer, E.; Viale, G.; Cameron, D.; Gianni, L. Triple-Negative Breast Cancer: Disease Entity or Title of Convenience. *Nat. Rev. Clin. Oncol.* **2010**, *7*, 683–692.
3. Liedtke, C.; Mazouni, C.; Hess, K. R.; Andre, F.; Tordai, A.; Mejia, J. A.; Symmans, W. F.; Gonzalez-Angulo, A. M.; Hennessy, B.; Green, M. Response to Neoadjuvant Therapy and Long-Term Survival in Patients with Triple-Negative Breast Cancer. *J. Clin. Oncol.* **2008**, *26*, 1275–1281.
4. Lorusso, P. M.; Canetta, R.; Wagner, J. A.; Balogh, E. P.; Nass, S. J.; Boerner, S. A.; Hohneker, J. Accelerating Cancer Therapy Development: the Importance of Combination Strategies and Collaboration. Summary of an Institute of Medicine Workshop. *Clin. Cancer Res.* **2012**, *18*, 6101–6109.
5. Barreto, J. A.; Malley, W.; Kubeil, M.; Graham, B.; Stephan, H.; Spiccia, L. Nanomaterials: Applications in Cancer Imaging and Therapy. *Adv. Mater.* **2011**, *23*, 18–40.
6. He, Q.; Shi, J. MSN Anti-Cancer Nanomedicines: Chemotherapy Enhancement, Overcoming of Drug Resistance, and Metastasis Inhibition. *Adv. Mater.* **2014**, *26*, 391–411.
7. Barua, S.; Mitragotri, S. Synergistic Targeting of Cell Membrane, Cytoplasm, and Nucleus of Cancer Cells Using Rod-Shaped Nanoparticles. *ACS Nano* **2013**, *7*, 9558–9570.
8. Liao, L.; Liu, J.; Dreaden, E. C.; Morton, S. W.; Shopsowitz, K. E.; Hammond, P. T.; Johnson, J. A. A Convergent Synthetic Platform for Single-Nanoparticle Combination Cancer Therapy: Ratiometric Loading and Controlled Release of Cisplatin, Doxorubicin, and Camptothecin. *J. Am. Chem. Soc.* **2014**, *136*, 5896–5899.
9. Li, F.; Zhao, X.; Wang, H.; Zhao, R.; Ji, T.; Ren, H.; Anderson, G. J.; Nie, G.; Hao, J. Multiple Layer-by-Layer Lipid-Polymer Hybrid Nanoparticles for Improved FOLFIRINOX Chemotherapy in Pancreatic Tumor Models. *Adv. Funct. Mater.* **2014**, 10.1002/adfm.201401583.
10. Liu, H.; Chen, D.; Li, L.; Liu, T.; Tan, L.; Wu, X.; Tang, F. Multifunctional Gold Nanoshells on Silica Nanorattles: A Platform for the Combination of Photothermal Therapy and Chemotherapy with Low Systemic Toxicity. *Angew. Chem., Int. Ed.* **2011**, *123*, 921–925.
11. You, J. O.; Guo, P.; Auguste, D. T. A Drug-Delivery Vehicle Combining the Targeting and Thermal Ablation of HER^{2+} Breast-Cancer Cells with Triggered Drug Release. *Angew. Chem., Int. Ed.* **2013**, *125*, 4235–4240.
12. Deng, Z. J.; Morton, S. W.; Ben-Akiva, E.; Dreaden, E. C.; Shopsowitz, K. E.; Hammond, P. T. Layer-by-Layer Nanoparticles for Systemic Codelivery of an Anticancer Drug and siRNA for Potential Triple-Negative Breast Cancer Treatment. *ACS Nano* **2013**, *7*, 9571–9584.
13. Jiang, T.; Mo, R.; Bellotti, A.; Zhou, J.; Gu, Z. Gel–Liposome-Mediated Co-Delivery of Anticancer Membrane-Associated Proteins and Small-Molecule Drugs for Enhanced Therapeutic Efficacy. *Adv. Funct. Mater.* **2014**, *24*, 2295–2304.
14. Deng, X.; Cao, M.; Zhang, J.; Hu, K.; Yin, Z.; Zhou, Z.; Xiao, X.; Yang, Y.; Sheng, W.; Wu, Y.; et al. Hyaluronic Acid-Chitosan Nanoparticles for Co-Delivery of MiR-34a and Doxorubicin in Therapy against Triple Negative Breast Cancer. *Biomaterials* **2014**, *35*, 4333–4344.
15. Singla, A. K.; Garg, A.; Aggarwal, D. Paclitaxel and Its Formulations. *Int. J. Pharm.* **2002**, *235*, 179–192.
16. Gelderblom, H.; Verweij, J.; Nooter, K.; Sparreboom, A. Cremophor EL: The Drawbacks and Advantages of Vehicle Selection for Drug Formulation. *Eur. J. Cancer* **2001**, *37*, 1590–1598.
17. Zheng, M.; Yue, C.; Ma, Y.; Gong, P.; Zhao, P.; Zheng, C.; Sheng, Z.; Zhang, P.; Wang, Z.; Cai, L. Single-Step Assembly of DOX/ICG Loaded Lipid–Polymer Nanoparticles for Highly Effective Chemo-Photothermal Combination Therapy. *ACS Nano* **2013**, *7*, 2056–2067.
18. Xu, Y.; Wang, J.; Li, X.; Liu, Y.; Dai, L.; Wu, X.; Chen, C. Selective Inhibition of Breast Cancer Stem Cells by Gold Nanorods Mediated Plasmonic Hyperthermia. *Biomaterials* **2014**, *35*, 4667–4677.
19. Shafirstein, G.; Bäumler, W.; Hennings, L. J.; Siegel, E. R.; Friedman, R.; Moreno, M. A.; Webber, J.; Jackson, C.; Griffin, R. J. Indocyanine Green Enhanced Near-Infrared Laser Treatment of Murine Mammary Carcinoma. *Int. J. Cancer* **2012**, *130*, 1208–1215.
20. Tam, J. M.; Tam, J. O.; Murthy, A.; Ingram, D. R.; Ma, L. L.; Travis, K.; Johnston, K. P.; Sokolov, K. V. Controlled Assembly of Biodegradable Plasmonic Nanoclusters for Near-Infrared Imaging and Therapeutic Applications. *ACS Nano* **2010**, *4*, 2178–2184.
21. Saxena, V.; Sadoqi, M.; Shao, J. Degradation Kinetics of Indocyanine Green in Aqueous Solution. *J. Pharm. Sci.* **2003**, *92*, 2090–2097.
22. Yoneya, S.; Saito, T.; Komatsu, Y.; Koyama, I.; Takahashi, K.; Duvoll-Young, J. Binding Properties of Indocyanine Green in Human Blood. *Invest. Ophthalmol. Visual Sci.* **1998**, *39*, 1286–1290.
23. Zaffaroni, N.; Pannati, M.; Diadone, M. G. Survivin as a Target for New Anticancer Interventions. *J. Cell. Mol. Med.* **2005**, *9*, 360–372.
24. Xu, G. C.; Zhang, P.; Leng, F.; Pan, L.; Li, Z. Y.; Yu, D. D.; Shan, Y.; Yuan, Q. Z.; Wen, Y.; Mu, B.; et al. Inhibition of Lymphatic Metastases by a Survivin Dominant-Negative Mutant. *Oncol. Res.* **2012**, *20*, 579–587.
25. Wang, H.; Wu, Y.; Zhao, R.; Nie, G. Engineering the Assemblies of Biomaterial Nanocarriers for Delivery of Multiple Theranostic Agents with Enhanced Antitumor Efficacy. *Adv. Mater.* **2013**, *25*, 1616–1622.
26. Guo, S.; Huang, Y.; Wei, T.; Zhang, W.; Wang, W.; Lin, D.; Zhang, X.; Kumar, A.; Du, Q.; Xing, J. Amphiphilic and Biodegradable Methoxy Polyethylene Glycol-block-(polycaprolactone-graft-Poly(2-(dimethylamino)ethyl Methacrylate)) as an Effective Gene Carrier. *Biomaterials* **2011**, *32*, 879–889.
27. Deshpande, M. C.; Davies, M. C.; Garnett, M. C.; Williams, P. M.; Armitage, D.; Bailey, L.; Vamvakaki, M.; Armes, S. P.; Stolnik, S. The Effect of Poly(ethylene glycol) Molecular Architecture on Cellular Interaction and Uptake of DNA Complexes. *J. Controlled Release* **2004**, *97*, 143–156.

28. Liu, Z.; Robinson, J. T.; Sun, X. M.; Dai, H. J. PEGylated Nanographene Oxide for Delivery of Water-Insoluble Cancer Drugs. *J. Am. Chem. Soc.* **2008**, *130*, 10876–10880.
29. Veronese, F. M.; Pasut, G. PEGylation, Successful Approach to Drug Delivery. *Drug Discovery Today* **2005**, *10*, 1451–1458.
30. Lutz, J. F.; Akdemir, O.; Hoth, A. Point by Point Comparison of Two Thermosensitive Polymers Exhibiting a Similar LCST: Is the Age of Poly (NIPAM) Over. *J. Am. Chem. Soc.* **2006**, *128*, 13046–13047.
31. Wang, H.; Zhao, Y.; Wu, Y.; Hu, Y. L.; Nan, K.; Nie, G.; Chen, H. Enhanced Anti-Tumor Efficacy by Co-Delivery of Doxorubicin and Paclitaxel with Amphiphilic Methoxy PEG-PLGA Copolymer Nanoparticles. *Biomaterials* **2011**, *32*, 8281–8290.
32. Nakayama, M.; Okano, T.; Miyazaki, T.; Kohori, F.; Sakai, K.; Yokoyama, M. Molecular Design of Biodegradable Polymeric Micelles for Temperature-Responsive Drug Release. *J. Controlled Release* **2006**, *115*, 46–56.
33. Liu, S. Q.; Tong, Y. W.; Yang, Y. Y. Incorporation and *in Vitro* Release of Doxorubicin in Thermally Sensitive Micelles Made from Poly(N-isopropylacrylamide-co-N,N-dimethylacrylamide)-b-poly(D,L-lactide-co-glycolide) with Varying Compositions. *Biomaterials* **2005**, *26*, 5064–7504.
34. Li, Y.; Wen, T.; Zhao, R.; Liu, X.; Ji, T.; Wang, H.; Shi, X.; Shi, J.; Wei, J.; Zhao, Y.; et al. Localized Electric Field of Plasmonic Nanoplatform Enhanced Photodynamic Tumor Therapy. *ACS Nano* **2014**, *8*, 11529–11542.